

Illuminating the Intrinsic Effect of Water Co-feeding on Methane Dehydroaromatization: A Comprehensive Study

Mustafa Çağlayan, Alessandra Lucini Paioni, Büşra Dereli, Genrikh Shterk, Idoia Hita, Edy Abou-Hamad, Alexey Pustovarenko, Abdul-Hamid Emwas, Alla Dikhtiarenko, Pedro Castaño, Luigi Cavallo, Marc Baldus, Abhishek Dutta Chowdhury, and Jorge Gascon*



Cite This: *ACS Catal.* 2021, 11, 11671–11684



Read Online

ACCESS |



Metrics & More



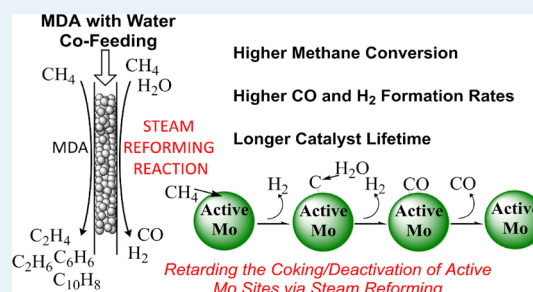
Article Recommendations



Supporting Information

ABSTRACT: Among all catalytic natural gas valorization processes, methane dehydroaromatization (MDA) still has a great potential to be utilized at an industrial level. Although the use of Mo/H-ZSM-5 as an MDA catalyst was first reported almost three decades ago, the process is yet to be industrialized, because of its inherent challenges. In order to improve the overall catalytic performance and lifetime, the co-feeding of water constitutes a promising option, because of its abundance and nontoxicity. Although water's (limited) positive influence on catalyst lifetime has earlier been exhibited, the exact course of action (like mechanism or the water effect on active sites) is yet to be established. To bridge this knowledge gap, in this work, we have performed an in-depth investigation to elucidate the effects of water co-feeding over a well-dispersed Mo/H-ZSM-5 catalyst by using an array of advanced characterization techniques (nuclear magnetic resonance (NMR), electron paramagnetic resonance (EPR), X-ray diffraction (XRD), X-ray photoelectron spectroscopy (XPS), thermogravimetry–temperature-programmed oxidation/mass spectroscopy (TG-TPO/MS), scanning transmission electron microscopy (STEM), N₂ physisorption, Raman spectroscopy, inductively coupled plasma–optical emission spectroscopy (ICP-OES)). Our results demonstrate that the addition of water results in the occurrence of steam reforming (of both coke and methane) in parallel to MDA. Moreover, the presence of water affects the reducibility of Mo sites, as corroborated with computational analysis to examine the state and locality of Mo sites under various water levels and transformation of the catalyst structure during deactivation. We anticipate that our comprehensive study of the structure–function relationship on Mo/H-ZSM-5 under humid MDA conditions will be beneficial for the development of future methane valorization technologies.

KEYWORDS: methane dehydroaromatization, water co-feeding, zeolites, bifunctional catalysts, heterogeneous catalysis



INTRODUCTION

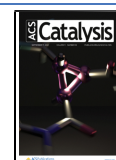
Methane, which is the main component of natural gas, could be a cleaner source of energy and raw material for the synthesis of carbon-based chemicals. The high transportation costs of natural gas, in comparison to other fossil fuels,¹ and the increasing anthropogenic methane emissions to the atmosphere (the concentration in 2018, 1857 ppb, is more than 2.5 times of levels in the pre-industrial era)² have stirred intense research on on-site conversion to condensed hydrocarbons (Scheme 1). Although several syngas-based indirect technologies were developed and commercialized, there is a great interest from both industry and academia for the development of direct routes for converting methane. From a different perspective, methane valorization presumably will be a future hot research topic, because of the strong worldwide efforts related to carbon capture and storage (CCS). Storing CO₂ underground inevitably would further increase the worldwide methane content in coming decades. Therefore, it is essential to derive direct catalytic methane valorization technologies to produce value-added liquid fuel and chemicals. However, such

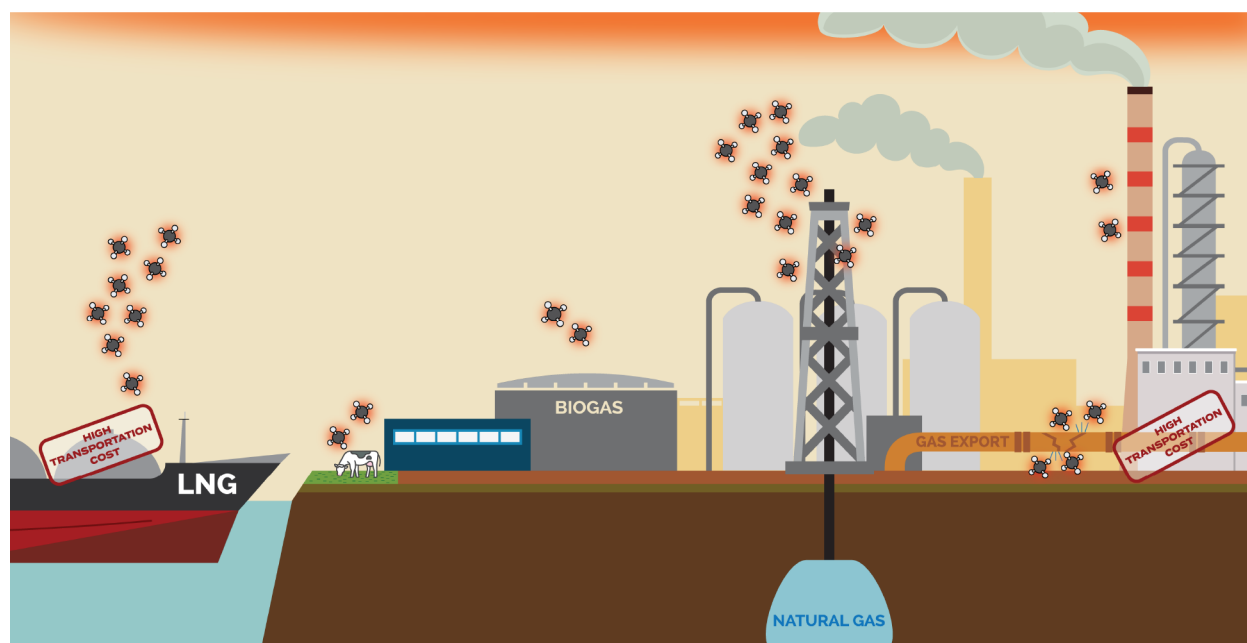
a direct conversion of methane is undoubtedly among the most important challenges in the catalytic science. This is mainly because of methane's thermochemical properties (i.e., high first bond dissociation energy (439.3 kJ/mol under standard conditions), small polarizability (2.84×10^{-40} C²m²/J), high ionization potential (12.6 eV), and high pK_a (~48)).³ Over the past decade, the most significant success was accomplished in the oxidative coupling of methane (OCM) by Siluria and Linde-Engineering.⁴ Besides OCM, research activities on the non-oxidative methane dehydroaromatization (MDA), first achieved on Mo incorporated ZSM-5 catalyst by Wang et al. in 1993,⁵ is currently also gaining momentum.^{1,6–10} Aromatics,

Received: June 20, 2021

Revised: August 15, 2021

Published: September 7, 2021



Scheme 1. Increasing Methane Emissions to the Atmosphere and the High Cost of Transportation^a

^aAlthough CH₄ emissions, the second-largest contributor to climate change, usually receive less attention than CO₂, recent reports^{2,13} are showing that immediate actions should be taken against it. In addition to this, high costs of gas transportation in comparison to other fossil fuels are causing a drawback for its off-site utilization.¹ Altogether, these issues make on-site conversion of methane to valuable chemicals and fuels an important topic for catalysis and reaction engineering communities.

having vast applications (gasoline additives, detergents, dyes, insecticides etc.), are mainly manufactured by crude oil refining in the modern chemical industry;¹⁰ however, MDA catalysis has a great potential to replace the existing processes since global natural gas (and biogas) production is increasing every year.¹¹ The major obstacle in front of this process is the quick and inevitable deactivation of Mo/ZSM-5 due to the high coke selectivity. To upgrade the process and catalyst for potential industrial applications, understanding the active site formation and the reaction network is of utmost importance. In a recent study from our group,¹² the direct C–C bond formation on Mo-incorporated ZSM-5 during the early stages of the reaction was evaluated via advanced solid-state NMR techniques; these observations reveal that both Mo-carbide and (methanol-to-hydrocarbons (MTH) like-) hydrocarbon pool (HCP)-driven methane conversion pathways coexist independently (involving both monofunctional and bifunctional features of the metal–zeolite catalyst). This understanding was developed by identifying acetylene (i.e., presumably the direct C–C bond-forming product from methane), methyldiene, allenes, acetal, and surface-formate species as other crucial intermediates.

As might be expected, to inhibit coking and improve the lifetime of MDA catalysis on Mo/ZSM-5, the addition of co-reactants (i.e., H₂, CO, CO₂, O₂, NO, and H₂O) has been considered in several earlier attempts.^{14–23} Overall, those attempts showed that these reagents can enhance the catalytic lifetime to some extent. In the case of oxidants, even though they can extend the deactivation period, it was found that their concentrations should not go beyond certain limits, because of three critical factors:^{17–19} (i) They can either poison the “activation period” or (ii) cause dealumination of the zeolite at high temperatures and, (iii) they may affect the type and spatial distribution of intermediates formed during the reaction

in an uncontrolled way. For instance; dimerization and cyclization reactions can be retarded due to the competitive adsorption between water and some olefins on Brønsted acid sites (BASs).²⁴ In the case of oxygen, the combustion of methane is difficult to prevent.²⁵ The addition of CO and/or CO₂ to the inlet stream was also found to have a narrow concentration range in which it can improve the catalyst lifetime of MDA.^{15,20} It was claimed that Boudouard reaction and dry-reforming were effective in the presence of CO₂. However, while co-feeding CO, the reported results are ambiguous, as reports vary from neutral to (not so significant) positive influence.^{15,20} The most recent CO co-fed studies^{14,23} reported that it slightly improves the durability of the catalyst through protecting MoC_x from being deactivated. The co-addition of hydrogen can suppress coking and extend the catalytic activity, but it may also decrease the formation rates of higher-molecular-weight hydrocarbons if it exceeds the critical concentration.^{20,22,26} In addition to the above-mentioned co-reactants, Bhan and colleagues tested some C_{1–2} hydrocarbons containing acid, carbonyl, and hydroxyl functional groups (i.e., acetic acid, ethanol, methanol, formic acid, acetaldehyde) as a co-feed in MDA catalysis.^{27–29} They found out that, in the upstream of catalytic bed, mainly oxygenate/CH₄ reforming occurs and CO is the only oxygen-containing product at the outlet. Besides, they spotted the oxidation of some active Mo sites during co-feeding and found a critical methane/oxygenate ratio for aromatics formation. Beyond all these investigations, there are other issues related to process safety and economics about co-feeding. For example; NO, CO, and H₂S are not desirable co-reactants for an industrial process because of their toxicity level. On the other side, H₂ and CO₂ may not be techno-economically feasible, in terms of their sources. Therefore, among the oxygenates listed above, H₂O comes to the forefront, because of its high abundance, low cost, and

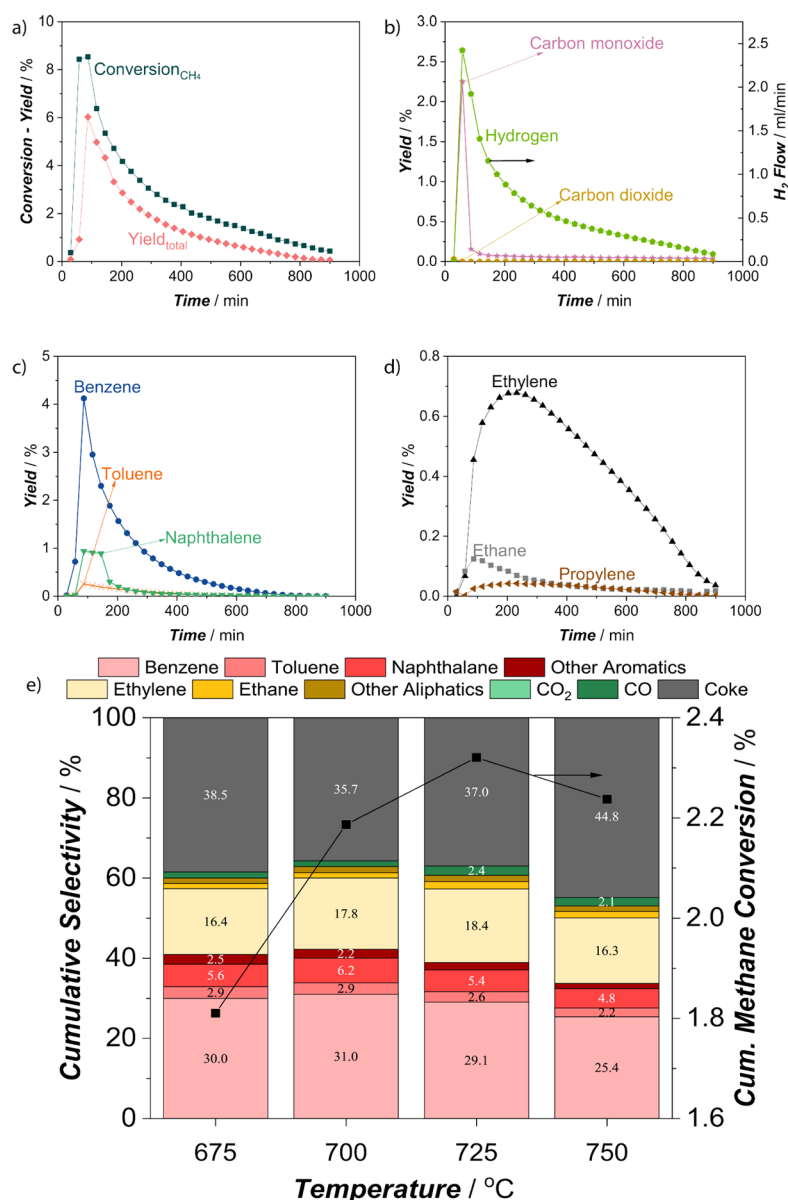


Figure 1. Catalytic activity of 2 wt % Mo/H-ZSM-5 (250 mg) in the absence of water (11.8 mol % N₂ and 88.2 mol % CH₄ in the inlet, total gas flow = 17 mL/min at STP) at atmospheric pressure: (a) conversion and total yield (without CO and CO₂) at 725 °C; (b) yields of CO, CO₂, and H₂ flow at 725 °C; (c) yields of major aromatic products (benzene, toluene, and naphthalene) at 725 °C; (d) yields of major aliphatic products (ethylene, ethane, and propylene) at 725 °C; and (e) cumulative hydrocarbon selectivities and cumulative methane conversion for 14-h performance test starting after the activation-induction period (after the second data point) at different temperatures. The data for the catalysis test at 725 °C are reproduced from our previous publication.¹²

nontoxicity. Although preliminary studies highlight the benefits of water addition (i.e., improving the catalyst lifetime),^{16,18,19} a proper structure–function relationship is lacking, which is necessary to maximize the product yield and increasing the economic impact of MDA process. In this work, besides analyzing the impact of water molecules on overall performance and catalyst structure (zeolite and Mo sites) with multimodal experimental (nuclear magnetic resonance (NMR), electron paramagnetic resonance (EPR), X-ray diffraction (XRD), X-ray photoelectron spectroscopy (XPS), thermogravimetry–temperature-programmed oxidation/mass spectroscopy (TG-TPO/MS), scanning transmission electron microscopy (STEM), N₂ physisorption, Raman spectroscopy, inductively coupled plasma–optical emission spectroscopy

(ICP-OES)) and computational methods, we also shed light on the influence of water and its reforming products on the hydrocarbon formation mechanisms, which was never studied previously, to this extent.

EXPERIMENTAL METHODS

Catalytic Activity Tests. All the catalytic performance tests, including the ones with labeled CH₄ (¹³CH₄ and CD₄), were performed in a fixed-bed reactor setup manufactured by PID Eng & Tech at atmospheric pressure, various temperatures, and humidity levels. (Please see the further details in Section S1.2 in the Supporting Information.) Regarding (1) methane conversion (%), (2) product yield for a specific product (%), (3) total yield (%) (not including CO and CO₂),

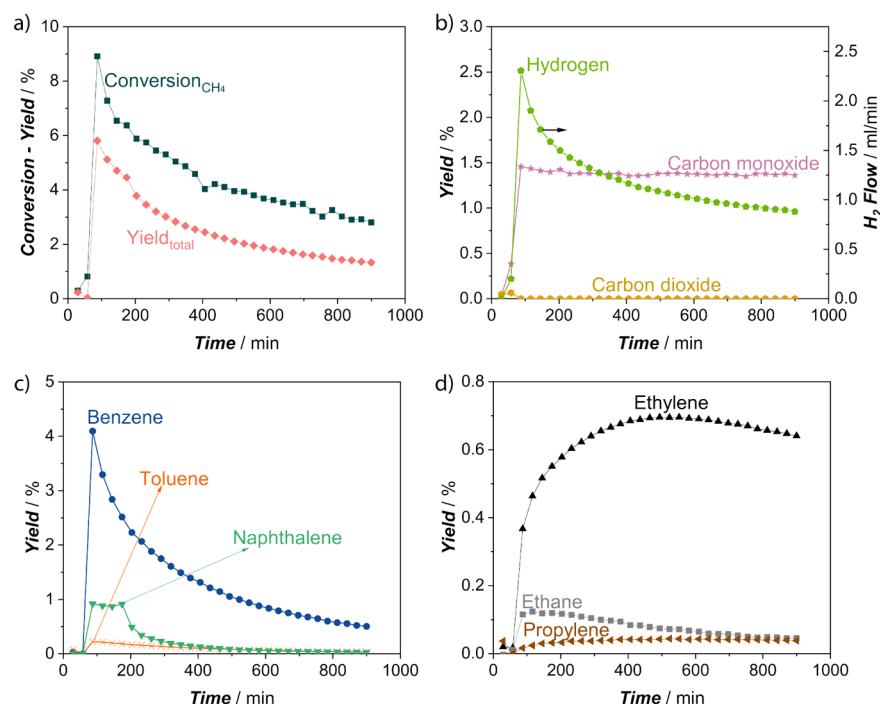


Figure 2. Catalytic activity of 2 wt % Mo/H-ZSM-5 (250 mg) under $P_{\text{H}_2\text{O}} = 0.020$ atm (11.8 mol % N_2 , 86.2 mol % CH_4 , and 2.0 mol % H_2O in the inlet; total gas flow = 17 mL/min at STP) at atmospheric pressure and 725 °C: (a) conversion and total yield (without CO and CO_2), (b) yields of CO, CO_2 , and H_2 flow, (c) yields of major aromatic products (benzene, toluene, and naphthalene), and (d) yields of major aliphatic products (ethylene, ethane, and propylene).

and (4) H_2 flow at the outlet (mL min^{-1} at STP), values were calculated as follows:

$$X_{\text{CH}_4} = \frac{F_{\text{CH}_4,\text{in}} - F_{\text{CH}_4,\text{out}}}{F_{\text{CH}_4,\text{in}}} \times 100 \quad (1)$$

$$Y_x = \frac{F_{x,\text{out}} \times (C_{\text{number of } x})}{F_{\text{CH}_4,\text{in}}} \times 100 \quad (2)$$

$$Y_{\text{total}} = \sum_{\text{All } x \text{ except CO, CO}_2} Y_x \quad (3)$$

$$F_{\text{H}_2,\text{out}} = y_{\text{H}_2,\text{out}} \times F_{\text{total,out}} \quad (4)$$

Catalyst Preparation and Characterization. A 2 wt % Mo/HZSM-5 catalyst was prepared via incipient wetness impregnation, following the method described in ref 12. All details about catalyst preparation and characterization are presented in the Supporting Information.

RESULTS AND DISCUSSION

Methane Dehydroaromatization Performance of Mo/ZSM-5. This comprehensive study was conducted on the material with a Mo loading of ca. 2 wt % and HZSM-5 with $\text{SiO}_2/\text{Al}_2\text{O}_3 = 26$. Dispersion of Mo and other important features of the catalysts were studied and confirmed by N_2 physisorption, Raman spectroscopy, XRD, STEM, ICP-OES, ^{27}Al -NMR, EPR, NH_3 TPD analyses (see the Supporting Information). In Figure 1, MDA performance of our catalyst in the absence of any co-feed is presented. As depicted, a low total product yield accompanied by high formation rates of CO and H_2 in the initial 60 min (the first two data points in

Figures 1a and 1b) indicates the reduction step of molybdenum sites, which is necessary for the MDA process.³⁰ After this period, the typical MDA activity of 2 wt % Mo/H-ZSM-5 catalyst becomes explicit. Total product yield (Y_{total}) and conversion (X_{CH_4}) reach their maximum values and then decay with time. The major aromatic and aliphatic product formation rates, with respect to time-on-stream (TOS) are presented in Figures 1c and 1d, respectively. In addition to the ones displayed in Figures 1c and 1d, more aromatic (i.e., *o*-xylene) and aliphatic (i.e., 1-butene/1,3-butadiene) species in the reactor effluent are detected, but their concentrations were relatively low. Figure 1e displays the performance of the model catalyst under non-oxidative conditions at 675, 700, 725, and 750 °C. The main differences among the experiments conducted at different temperature levels are the initial activity and deactivation time: The higher the reaction temperature becomes, the faster the deactivation gets, and the higher initial activity occurs (see Figures S5 and S6 in the Supporting Information). For all temperature levels, the major contribution to total product yields comes from the aromatics (Figure 1e). Under these conditions (catalyst amount, space velocity, time on stream, etc.), the optimal temperature is found as 725 °C; since it has the highest cumulative methane conversion and ~60% cumulative selectivity to aromatics and aliphatics after 14 h of MDA catalysis.

Effect of Water Co-feeding on MDA Catalysis. As a next step, we investigated the effect of water and its concentration on the catalysis performance at 725 °C. When we introduced ca. 2.0 vol % water to the inlet stream; major valuable product yields were not only elevated but also improved, in terms of production lifetime (Figure 2). Another difference noticed between the two cases (in the absence and

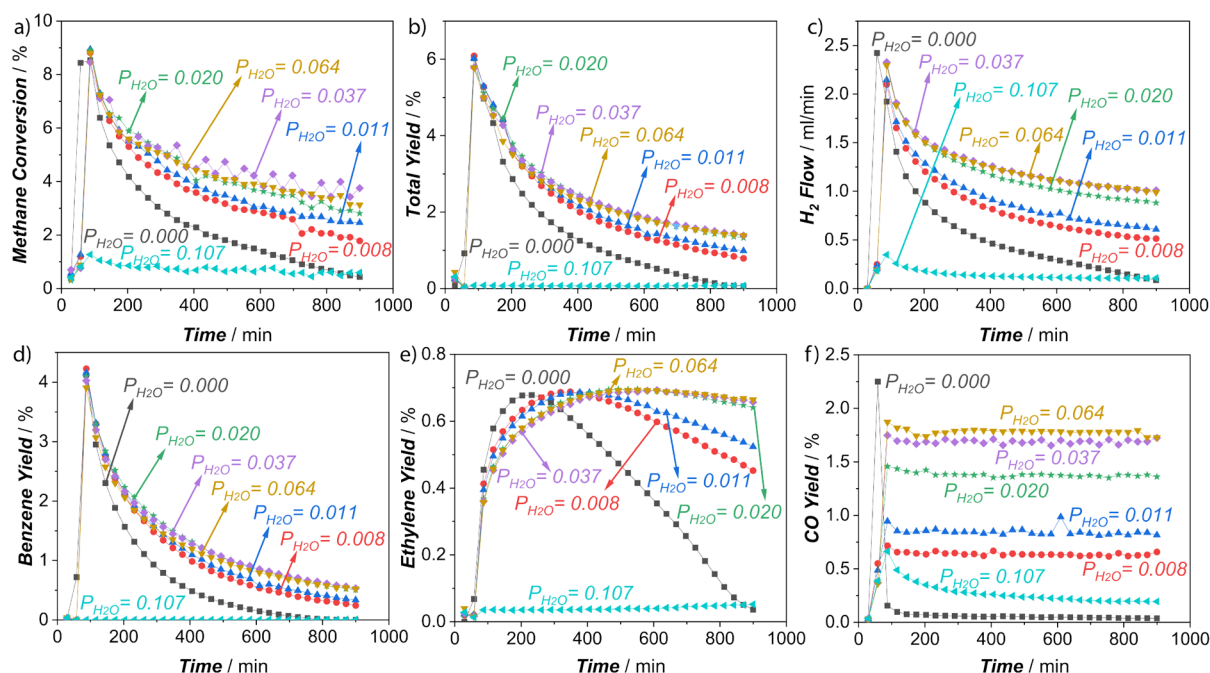


Figure 3. Catalytic activity of 2 wt % Mo/H-ZSM-5 (250 mg) under different water concentrations (given in the graph as partial pressure, atm) at atmospheric pressure and 725 °C: (a) methane conversion, (b) total yield (without CO and CO₂), (c) H₂ flow, (d) benzene yield, (e) ethylene yield, and (f) CO yield.

in the presence of a 2 vol % water) is the methane conversion levels (see Figures 1a and 2a). It can be clearly seen that, along with the aromatic and aliphatic hydrocarbons, a significant contribution to higher conversion level upon the addition of water is derived from the formation of CO (Figure 2b). Indeed, CO production remains in this case constant during the reaction while all other hydrocarbon yields (Figures 2c and 2d) change with time. These results indicate that CO production is independent of the MDA reaction network and suggests that reforming reactions ($\text{CH}_4 + \text{H}_2\text{O} \rightleftharpoons \text{CO} + 3\text{H}_2$ overall) occur parallel to dehydroaromatization (Section S2.2 in the Supporting Information). Furthermore, the absence of CO₂ (Figure 2b) at the outlet after the induction period suggests that the water–gas shift reaction (highly equilibrium limited at 725 °C) does not contribute to the products significantly, which is consistent with previous reports.^{20,31,32} Furthermore, the in situ formed CO molecules, as a result of reforming reactions, may contribute to the enhancement of catalysis performance through protecting active Mo sites from being quickly deactivated, because of the coke deposition on it (via CO dissociation).^{14,23} To confirm this feature of CO, we performed additional CO co-feeding experiments. Although CO is not being consumed during the process (except the activation period), we have observed improvement in the product yields and slight enhancement on the catalyst lifetime (see Figures S18 and S19 in the Supporting Information), in comparison to conditions without any co-feeds. (Please see the further discussions in Section S2.3.3 in the Supporting Information). When it comes to the formation of hydrogen (Figure 2b), it can be formed both via reforming and MDA. Based on the earlier studies, hydrogen co-fed to MDA reaction does not promote the conversion of methane, but it can mitigate coke formation responsible for the catalyst deactivation.²⁵ Therefore, the increase in hydrogen concentration (co-product of steam reforming) may contribute to the process by

hydrogasification and/or preventing excessive dehydrogenation of some intermediates/products.^{33,34} To further gain insights into the effect of water, we have performed a control experiment by changing the reactant to ²H-isotope-enriched CD₄ from CH₄ (see Figure S45 in the Supporting Information). Herein, we intended to perform ¹H NMR experiments to track ¹H coming solely from the co-fed water. However, it is a complicated attempt, as zeolites are highly hygroscopic and have a tendency to give a broad proton spectrum. Also, any special sample treatment (like drying the sample prior to the measurement) is not an option here, as we intend to track water down in the sample. Apparently, no significant differences in 1D ¹H NMR spectra of samples have been observed under both dry and wet conditions at both 50 min and 2 h (see Figures S45a–c). Still, it is worth highlighting the well-defined resonance at ~7 ppm, which is already visible after a 50 min reaction for the dry sample, contrary to the wet sample case. Considering its relatively narrow resonance, this peak could be attributed to mobile aromatics. Moreover, the aromatic species resolved well only after the 2 h of reaction in the case of the wet sample, which essentially provides more justification of its lesser sensitivity than the dry sample. In order to have more-accurate information, the ¹H–¹H DQ-SQ experiment³⁵ has been performed to demonstrate that co-fed water only contributed (albeit small) to the formation of the aliphatic part of the zeolite-trapped organics (see Figure S45d).

The same catalyst (2 wt % Mo/H-ZSM-5) was tested under various water concentrations at 725 °C (Figure 3). It was observed that water positively influences the product yields and methane conversion up to some water level ($P_{\text{H}_2\text{O}} = 0.037$ atm). The yields of all products (i.e., benzene, ethylene, and CO) (Figures 3d–f) were improved significantly, and there was a keen increase in hydrogen formation (Figure 3c) up to a H₂O concentration of ca. 3.7 vol %; however, these were not continued beyond that point (Figure 3). When the water

concentration in the inlet stream increased to ca. 10.7 vol %, MDA catalysis was harshly inhibited. As depicted in Figures 3d and 3e, benzene and ethylene, two important products of MDA, became almost negligible under this condition. In this case, we detected only benzene, ethylene, ethane, CO, and CO₂ in the reactor effluent; other species (i.e., toluene, propylene, etc.) observed in lower water levels were not detected. Surprisingly, the obtained ethane yield in this experiment (Figure S10a in the Supporting Information) was comparable to the other experiments, in terms of order of magnitude. These results suggest that (i) for the formation of ethane–ethylene, one does not need a fully activated catalyst (complete Mo reduction and induction period); the partially reduced Mo sites (see Figure S25b and Table S6 in the Supporting Information) can form C₂ molecules from methane. This is also in agreement with Beale et al.,³⁶ where they reported that partially reduced metastable Mo sites can achieve methane coupling. Moreover, most likely, detected low benzene formation under $P_{\text{H}_2\text{O}} = 0.107$ atm resulted from the cyclization of C₂s on BASs. (ii) Since most of the Mo sites are not completely activated (vide infra, see Sections S2.6 and S2.9 in the Supporting Information), it is expected that the dehydrogenation on Mo sites would be hampered, and many oligomerization products would disappear. Consistent with this, in comparison to other conditions, we observed a significantly high ethane/ethylene ratio under 10.7 vol % water concentration (see Figure S13 in the Supporting Information). These results suggest that ethane is the primary methane activation product in MDA catalysis, and ethylene forms via its dehydrogenation, as proposed by Bhan et al.³⁷ Besides, the sharp decrease in H₂ and CO formation under 10.7 vol % water concentration (see Figures 3c and 3f) also implies that a high water level is detrimental for steam-reforming reactions. Furthermore, the cumulative product yields and conversion for all conditions were calculated to find the optimal humidity level at 725 °C for 14-h catalytic test (Figure 4). The total methane conversion was significantly enhanced and made a peak point at ~3.7 vol %. However, one

should be careful with the water concentration, because as it increases, the total selectivity of valuable hydrocarbons (aliphatics and aromatics) starts decreasing significantly and CO is becoming the dominant product (Figure 4). Altogether, these show that there should be a limiting water concentration, as Ichikawa and colleagues suggested.¹⁹ When this limit is crossed, the reduction of Mo is hampered and, thus, the active sites to achieve MDA are not formed. As previously stated, the steam-reforming reaction was also retarded under a H₂O concentration of 10.7 vol %; this implies that, not only for MDA but also for steam-reforming activity, one needs reduced Mo sites on the zeolite. To confirm this, we performed an experiment in which we fed dry methane until the end of the activation/induction period (which is approximately the initial 60 min of the experiments), and afterward we switched to the stream having high water concentration ($P_{\text{H}_2\text{O}} = 0.107$ atm) (see Figure S14 in the Supporting Information). We observed that, after dry treatment, a H₂O concentration of 10.7 vol % did not retard MDA and reforming reactions; typical MDA performance was detected. Overall, this portrays that water/methane ratio is a critical parameter for the activation of the Mo sites.

To understand the temperature effect, other temperature levels were studied under the same humidity level ($P_{\text{H}_2\text{O}} = 0.020$ atm). (The detailed product distributions are presented in Figures S7–S9 in the Supporting Information.) While water significantly enhanced the overall hydrocarbon formation and catalyst stability at temperatures equal/above 700 °C, it was detrimental to the activity of the catalyst at 675 °C. This showed that each temperature level has a distinct water range in which we can activate the catalyst, and the upper limit increases with increasing temperature. The yields of MDA products and the catalysis lifetime were improved at 700, 725, and 750 °C under a H₂O concentration of 2.0 vol % in comparison to their corresponding dry counterparts. However, CO yield was not affected by the temperature change, same for all three temperature levels and almost constant after the activation–induction period. One may argue that, at these three temperature levels, we might have already converted all the water in the inlet; this can be the reason for the unchanging CO yields. However, there is an important finding rejecting this argument. By changing our catalyst with ones having a higher SAR ratio (371) and/or higher Mo amount, we observed that CO yield under a value of $P_{\text{H}_2\text{O}} = 0.020$ atm significantly varied (see Figure S12 and Table S2 in the Supporting Information). This indicates that the Mo concentration and its distribution on/in the zeolite have great importance for the steam reforming reaction. For the scope of this study, we excluded the influence of Mo amount/distribution, since it requires further intensive investigations.

It is obvious that the formation rate of major aromatic and aliphatic products is increased upon the addition of water in a certain inlet composition. However, the trend of increase in yield of a specific product does not need to be the same with others. To understand what is changing with respect to inlet water concentration, we calculated yield ratios between some key products identified in the effluent gas (Figure 5). If one of the species has higher increase in its yield in comparison to others, its formation affinity is higher than the others. As depicted in Figures 5a–c, ethane/ethylene, ethane/C₄ (1-butene + 1,3-butadiene), and ethane/propylene yield ratios increase with the inlet water concentration. Clearly seen from

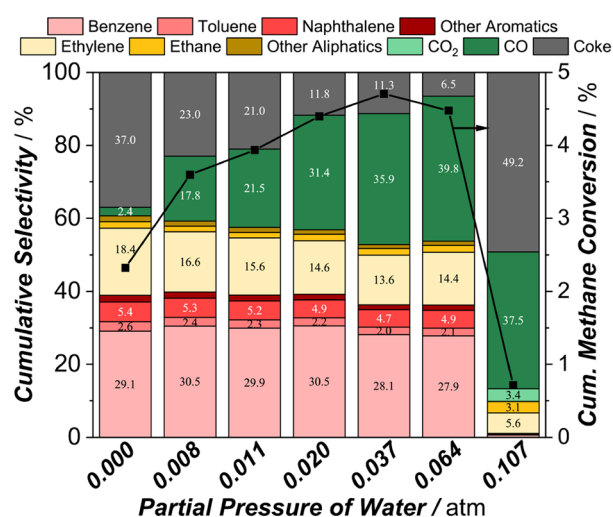


Figure 4. Cumulative hydrocarbon selectivities and cumulative methane conversion on 2 wt % Mo/H-ZSM-5 (250 mg) for 14-h performance test starting after the induction period (after the 2nd data point) under different water concentrations (given in the graph as partial pressure, atm) at atmospheric pressure and 725 °C.

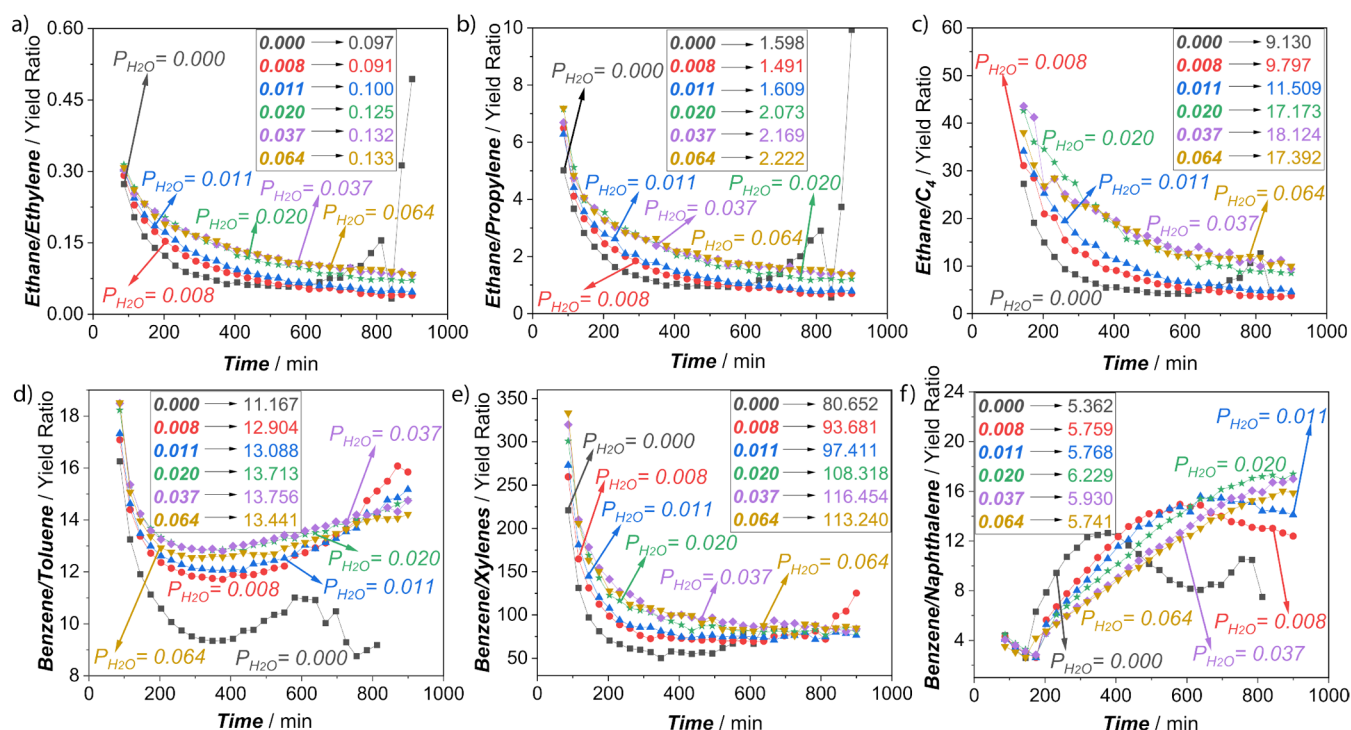


Figure 5. (a) Ethane/ethylene, (b) ethane/propylene, (c) ethane/ C_4 (1-butene + 1,3-butadiene), (d) benzene/toluene, (e) benzene/xylenes, (f) benzene/naphthalene yield ratios for the catalysis tests performed with 2 wt % Mo/H-ZSM-5 (250 mg) under different water concentrations (given in the graph as partial pressure, atm) at atmospheric pressure and 725 °C. The inset tables are cumulative yield ratios for 14-h performance tests starting after the induction period.

Figures 5a–c, increasing the inlet water concentration after some point does not improve the ethane related yield ratios. The yield ratios for benzene/toluene and benzene/xylenes (Figures 5d–f) also increase, with respect to the water level. Similar to the ethane case, benzene formation affinity is higher than toluene and xylene formation affinities, despite the enhancement in the overall net production rates (Figure 4). In the case of benzene/naphthalene ratio, it is slightly complicated to assess the data. Based on the cumulative benzene/naphthalene ratio (inset table in Figure 5f), benzene is becoming more favorable with the water introduction. When it comes to time-dependent data (Figure 5f), there are two different regions. In the initial periods of the catalysis, benzene/naphthalene ratio is decreasing with the water level. This means that steam-reforming enhances the net naphthalene formation rate more strongly than the net benzene formation rate in the early periods. Nevertheless, as the system approaches toward the deactivation, the ratio starts flipping around; and benzene production affinity is becoming higher than naphthalene production affinity with the increase in inlet water concentration (see Section S2.3.1 in the Supporting Information). One of the reasons for these trends might be the higher concentration of H_2 , which is not only formed as a product of methane aromatization but through the reforming of CH_4 .^{16,27} To validate this, we performed H_2 co-feeding experiment (see Figure S15 in the Supporting Information) and compared the yield ratios with H_2O co-feeding data. For the yield ratios presented in Figure 5, water and hydrogen result in very similar trends (Figure S16 in the Supporting Information). The only difference observed was the benzene/ethylene ratio. While H_2O co-feeding slightly improved benzene/ethylene ratio, the H_2 co-feed did not have a positive influence (Figure S17b in the Supporting Information). Aside

from H_2 , CO co-feeding experiment also exhibits very similar trends (Figure S20 in the Supporting Information); including benzene/ethylene ratio (Figure S20e). Since CO's main effect on MDA catalysis is protecting the active Mo sites from the fast deactivation via dissociation on them (see Section S2.3.3), these results imply that stability and structure of active Mo sites play a key role in distribution of the products and formation affinities. Also, these collectively reveal that different co-adjuvants may have different effects on active sites. In terms of aromatization, while both H_2O and CO co-feeding delivered positive influence on benzene/ethylene ratio, H_2 's role is almost neutral. Furthermore, it should be noted that water molecules can occupy BASs/form hydronium ions, thus there might be changes in the extent of BAS-assisted dimerization/cyclization steps and consequent hydrocarbon pool mechanism.³⁸

Effect of Water Co-feeding on Hydrocarbon Formation Mechanism. In order to provide more in-depth mechanistic information, advanced “mobility-dependent” magic angle spinning (MAS) solid-state NMR (ssNMR) spectroscopy was performed on post-reacted 2 wt % Mo/H-ZSM-5 material after the MDA reaction at 725 °C, using fully ^{13}C -enriched methane ($^{13}CH_4$) reactant (please see section S2.10.1 in the Supporting Information for detailed discussion). In this work, only the $P_{H_2O} = 0.020$ -spent sample has been included, since, very recently, we have reported a ssNMR-based mechanistic investigation on its $P_{H_2O} = 0.000$ -counterpart.¹² The 1H – ^{13}C cross-polarization (CP),³⁹ 1H – ^{13}C insensitive nuclei enhanced by polarization transfer (INEPT),⁴⁰ and ^{13}C direct excitation (DE) ssNMR spectra of the spent $P_{H_2O} = 0.020$ _2 h catalyst displayed a response originating from unsaturated hydrocarbons (aromatics and

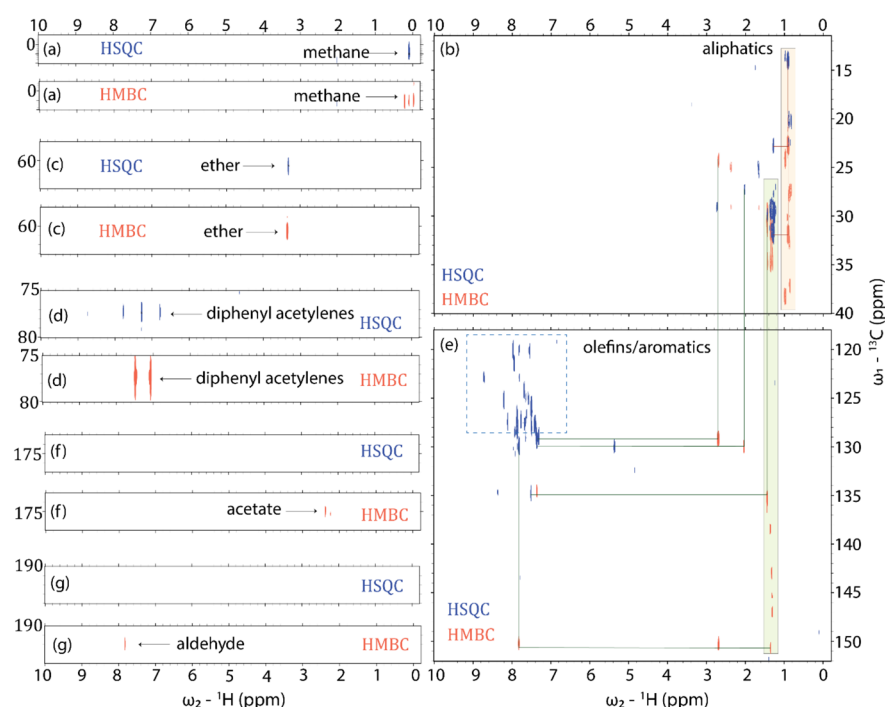


Figure 6. ^1H – ^{13}C heteronuclear single quantum coherence (HSQC, in blue) and heteronuclear multiple bond correlation (HMBC, in red) spectra, highlighting the presence of (a) unreacted methane molecules, (b) aliphatic region, (c) ether species, (d) alkynes (possibly direct C–C bond containing species), (e) unsaturated hydrocarbons region (olefinic/aromatics species), (f) acetate, and (g) aldehyde species. The spectra were obtained after (^{13}C)–methane dehydroaromatization reaction over 2 wt % Mo/H-ZSM-5 at atmospheric pressure and 725 °C under $P_{\text{H}_2\text{O}} = 0.020$ atm (11.8 mol % N_2 , 86.2 mol % $^{13}\text{CH}_4$ and 2.0 mol % H_2O in the inlet, total gas flow = 17 mL/min at STP) for 2 h, followed by acid dissolution of post-reacted catalysts and subsequent extraction to organic solvent (CDCl_3).

olefins) and adsorbed methane only (see Figure S40 in the Supporting Information), which is similar to our previous results on dry samples.¹² Both 2D ^{13}C – ^1H and ^{13}C – ^{13}C correlation spectra collectively revealed (see Figures S41 and S42 in the Supporting Information), the existence of zeolite-trapped (rigid and mobile) alkylated olefinic/(poly)aromatic species and numerous adsorbed forms of unreacted methane.^{41–45} Moreover, the existence of surface-formate species (cf. 170–173 ppm (^{13}C)/~8 ppm (^1H)) further provides support in favor of Koch-type carbonylation mechanism during the MDA process under wet conditions too.^{12,46} Although the utilization of a fully isotope-enriched reactant increased the NMR signal intensities and allowed us to perform multi-dimensional ssNMR correlation experiments for the structural elucidation of the zeolite-trapped species, the sensitivity of post-reacted wet samples has not been fully satisfactory. Thus, we have decided to perform the acid dissolution of post-reacted materials and subsequently perform liquid NMR after extracting the organics from acid to organic phase (i.e., the so-called “Guinset method”).⁴⁷

2D HSQC (Heteronuclear Single Quantum Correlation)⁴⁸ and HMBC (Heteronuclear Multiple Bond Correlation)⁴⁹ proton-detected NMR experiments are performed to probe the ^1H / ^{13}C one-bond connectivity and the ^1H / ^{13}C multiple-bond connectivity, respectively. As shown in Figure 6, in the ^1H – ^{13}C one-bond correlation experiment (blue spectrum), the presence of aliphatic (1–3 ^1H ppm/16–31 ^{13}C ppm) and aromatic (6–8.5 ^1H ppm/120–150 ^{13}C ppm) signals can be readily identified. By combining the HSQC and the HMBC spectra, we recognize the aliphatic resonances that belong to the same molecules (peaks connected by maroon lines).

Moreover, in the HMBC (orange spectrum), at a resonance characteristic of methyl protons corresponds different carbon signals of methyl and ethyl groups (highlighted in the yellow box), revealing the presence of various branched paraffins. In a similar way, we can also identify correlations between aliphatic and aromatic signals (connected by dark green lines), as well as aromatic carbons with a proton chemical shift characteristic of aliphatic resonances, clearly showing the presence of methylated (poly)aromatics and/or methylated olefins. However, the majority of the aromatic moieties are non-substituted aromatics (blue dotted box).

Methane signal was also probed in both experiments, together with peaks corresponding to ether signals and diphenyl acetylenes (Figure 6). Interestingly, additional resonances are observed in the ^1H – ^{13}C multiple-bond correlation experiment. For instance, a peak at 45 ppm ^{13}C and 0.87 ppm ^1H could indicate an interaction with a Brønsted acidic OH group of the zeolite. Moreover, the 175 (^{13}C)/ 2.38 (^1H) resonance is indicative of acetate moieties and the signal with 192 ppm ^{13}C /7.8 ppm ^1H chemical shift possibly corresponds to aromatic aldehyde.

Effect of Water Co-feeding on Catalyst Structure.

Since water was not heavily incorporated into the zeolite-trapped organics, it eventually prompted us to investigate the effect of co-fed water on the catalytic material itself. Under our reaction conditions, it is well-known that the water could dealuminate the zeolite material. Therefore, to probe the local atomic environment of aluminum and to monitor zeolite’s structural change during the reaction under different water levels, both 1D ^{27}Al MAS NMR and 2D ^{27}Al multiple-quantum (MQ) MAS NMR were performed (please see section S2.10.2,

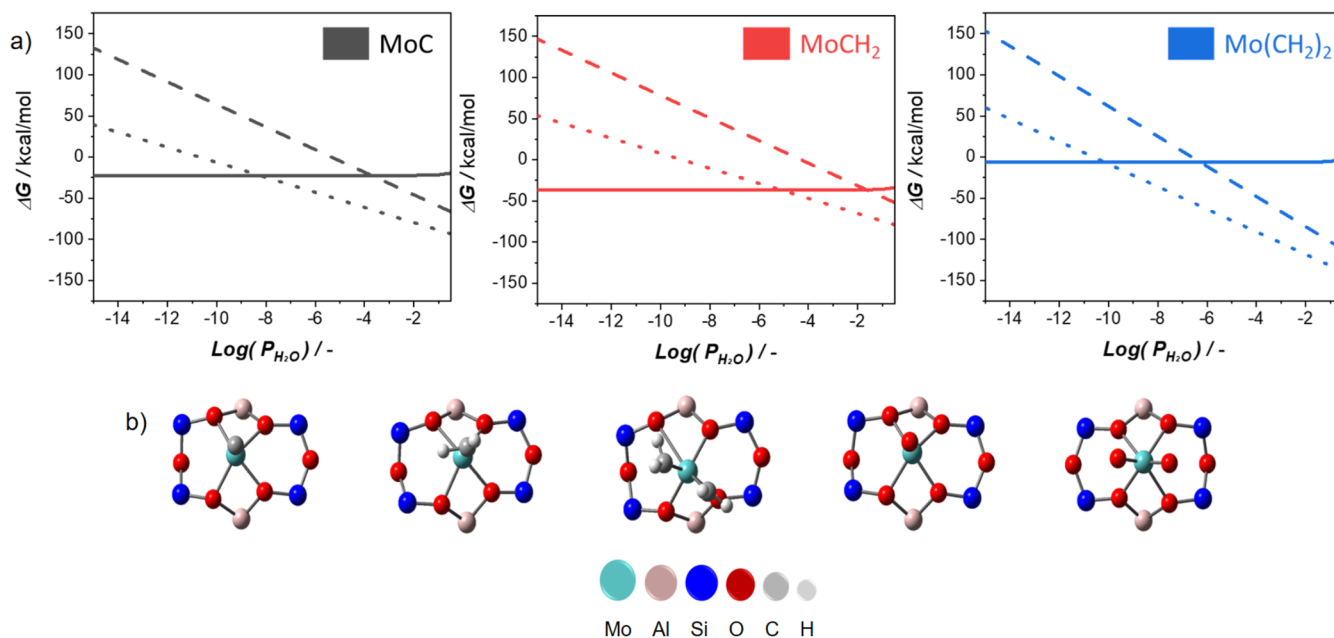


Figure 7. (a) Free-energy profiles at 725 °C for monomeric Mo species, as a function of H₂O partial pressure: the solid lines (—) represent the “reduction from MoO₂” ($\text{MoO}_2 + (x + 2)\text{CH}_4 \leftrightarrow \text{MoC}_x\text{H}_y + 2\text{CO} + 2\left(2 + x - \frac{y}{4}\right)\text{H}_2$); the dashed lines (---) represent the “oxidation to MoO₂” ($\text{MoC}_x\text{H}_y + (2 + x)\text{H}_2\text{O} \leftrightarrow \text{MoO}_2 + x\text{CO} + \left(2 + x + \frac{y}{2}\right)\text{H}_2$); and the dotted lines (···) represent the “oxidation to MoO” ($\text{MoC}_x\text{H}_y + (1 + x)\text{H}_2\text{O} \leftrightarrow \text{MoO} + x\text{CO} + \left(1 + x + \frac{y}{2}\right)\text{H}_2$); $P_{\text{CO}} = 10^{-2.0}$ atm, $P_{\text{H}_2} = 10^{-2.0}$ atm, $P_{\text{N}_2} = 0.11$ atm, $P_{\text{CH}_4} = 1 - P_{\text{CO}} - P_{\text{H}_2} - P_{\text{N}_2} - P_{\text{H}_2\text{O}}$. (b) Shorthand structures of DFT optimized cluster models (from left to right: MoC, MoCH₂, Mo(CH₂)₂, MoO, and MoO₂) for mononuclear Mo species used in free-energy analysis. For further details, see Section S3.4 in the Supporting Information.

Figures S46 and S47, in the Supporting Information). For the fresh catalyst, in addition to the typical tetra-, penta-, and octahedral Al sites, Anderson-type aluminum polyoxymolybdates ($\text{Al}(\text{OH})_6\text{Mo}_6\text{O}_{18}$) were observed at ~12 ppm after Mo introduction. Not detecting these species by XRD and Raman spectroscopy is suggesting that they were well-dispersed in/on zeolite particles. In the case of spent catalysts ($P_{\text{H}_2\text{O}} = 0.000$, 0.020, and 0.107 atm), a higher degree of heterogeneity and a wider distribution in isotropic chemical shifts were observed: For the catalysts spent under wet conditions, a significant degree of distortion for the six-coordinated Al species (EFAL) was detected while EFAL was almost negligible on the $P_{\text{H}_2\text{O}} = 0.000$ -spent material. Via MQMAS analysis, we also observed anisotropy of the tetrahedral Al signal, which can be correlated to the presence/amount of water in the catalysis experiments.

Furthermore, we evaluated basic crystallographic characteristics of the catalysts reacted under different humidity levels at 725 °C via XRD/Pawley analyses (see Section S2.11 in the Supporting Information). Comparing the diffractograms of spent catalysts with its fresh predecessor, we observed gradual disappearance of characteristic doublets of ZSM-5 (in the range of 23.0°–23.5° and 45.0°–46.0°) as the level of humidity decreases. It was also noticed that the unit-cell dimensions evaluated applying Pawley refinement protocol were significantly distorted upon deactivation. Besides, STEM images of spent catalysts (Figures S27–S29 in the Supporting Information) depict the formation of Mo nanoparticles. Especially $P_{\text{H}_2\text{O}} = 0.107$ -spent samples (see Figure S29) represents a much higher density of Mo nanoparticles in comparison to $P_{\text{H}_2\text{O}} = 0.020$ -spent and $P_{\text{H}_2\text{O}} = 0.000$ -spent (see

Figures S27 and S28). Noteworthy, the emergence of Mo agglomerates is not detectable on the XRD patterns, regardless of the reaction conditions to which they were exposed, which indicates their amorphous nature.

Another vital point is the water effect on molybdenum sites. Via XPS, only Mo⁶⁺ features are detected on the fresh catalyst (see Figure S25a in the Supporting Information), but thanks to the sensitivity of EPR spectroscopy, the presence of Mo⁵⁺ in the pristine catalyst was observed as well ($g = 1.9731$). (See the discussion in Section S2.9 in the Supporting Information.) By applying XPS spectroscopy on the spent catalysts ($P_{\text{H}_2\text{O}} = 0.000$, 0.020, and 0.107 atm), it was seen that most of Mo⁶⁺ sites were reduced (see Figure S25b in the Supporting Information). Comparing the spectra for $P_{\text{H}_2\text{O}} = 0.000$ -spent and $P_{\text{H}_2\text{O}} = 0.020$ -spent samples made us conclude that, in terms of molybdenum reduction and activity, there is no difference between the dry case and the wet cases (excluding $P_{\text{H}_2\text{O}} = 0.107$), but the water molecules are delaying the fast reduction/deactivation of Mo sites, which is enhancing the catalysis performance. When it comes to the XPS data for $P_{\text{H}_2\text{O}} = 0.107$ -spent sample, lower oxidation states identified in the other two samples (i.e., Mo²⁺) were not detected, which explains the negligible MDA activity. Besides, Mo⁵⁺ species were detected on the catalysts spent under wet conditions (especially $P_{\text{H}_2\text{O}} = 0.107$) via EPR ($g = 1.9402$; see Figure S39 in the Supporting Information). This is most likely related to the defects in Mo clusters formed on the external surface during the process.

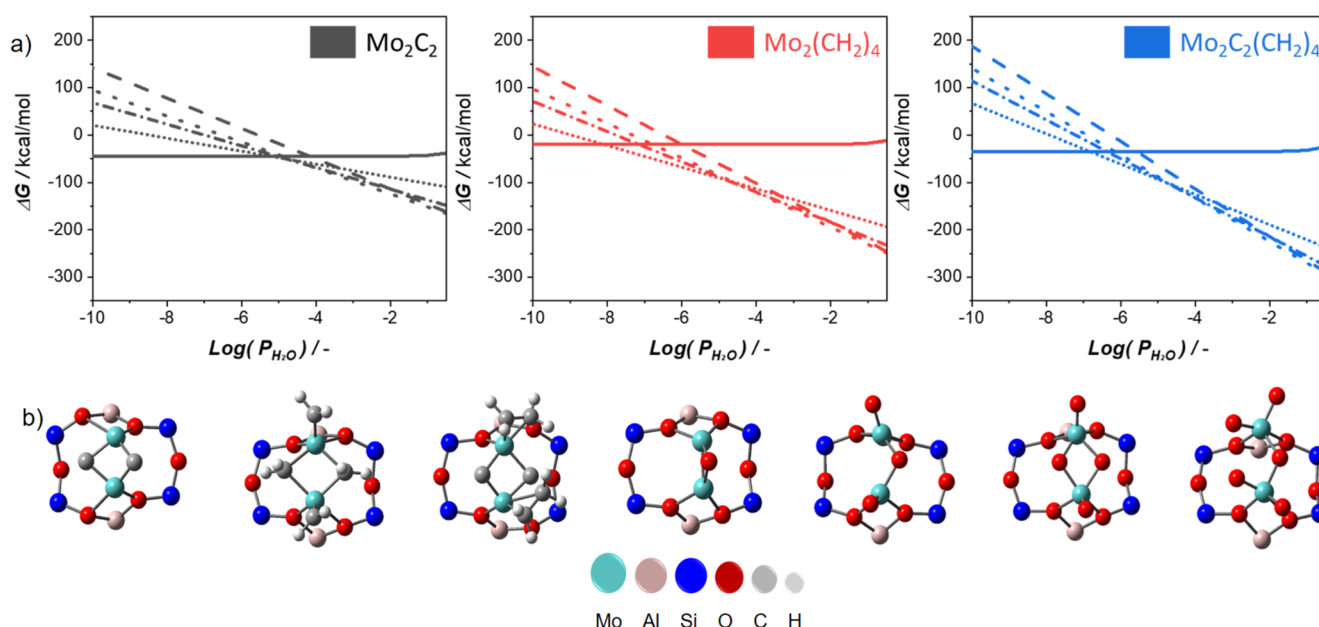


Figure 8. (a) Free-energy profiles at 725 °C for dimeric Mo species oxidation as a function of H₂O partial pressure: the solid lines (—) represent the “reduction from Mo₂O₅” ($\text{Mo}_2\text{O}_5 + (x + 5)\text{CH}_4 \leftrightarrow \text{Mo}_2\text{C}_x\text{H}_y + 5\text{CO} + 2\left(5 + x - \frac{y}{4}\right)\text{H}_2$); the dashed lines (---) represent the “oxidation to Mo₂O₅” ($\text{Mo}_2\text{C}_x\text{H}_y + (5 + x)\text{H}_2\text{O} \leftrightarrow \text{Mo}_2\text{O}_5 + x\text{CO} + \left(5 + x + \frac{y}{2}\right)\text{H}_2$); the loosely dotted lines (···) represents “oxidation to Mo₂O₄” ($\text{Mo}_2\text{C}_x\text{H}_y + (4 + x)\text{H}_2\text{O} \leftrightarrow \text{Mo}_2\text{O}_4 + x\text{CO} + \left(4 + x + \frac{y}{2}\right)\text{H}_2$); the dashed-dotted lines (- · -) represents “oxidation to Mo₂O₃” ($\text{Mo}_2\text{C}_x\text{H}_y + (3 + x)\text{H}_2\text{O} \leftrightarrow \text{Mo}_2\text{O}_3 + x\text{CO} + \left(3 + x + \frac{y}{2}\right)\text{H}_2$); and the densely dotted lines (····) represents “oxidation to Mo₂O” ($\text{Mo}_2\text{C}_x\text{H}_y + (1 + x)\text{H}_2\text{O} \leftrightarrow \text{Mo}_2\text{O} + x\text{CO} + \left(1 + x + \frac{y}{2}\right)\text{H}_2$); $P_{\text{CO}} = 10^{-2.0}$ atm, $P_{\text{H}_2} = 10^{-2.0}$ atm, $P_{\text{N}_2} = 0.11$ atm, $P_{\text{CH}_4} = 1 - P_{\text{CO}} - P_{\text{H}_2} - P_{\text{N}_2} - P_{\text{H}_2\text{O}}$. (b) Shorthand structures of DFT optimized cluster models (from left to right: Mo₂C₂, Mo₂(CH₂)₄, Mo₂C₂(CH₂)₄, Mo₂O, Mo₂O₃, Mo₂O₄, and Mo₂O₅) for dinuclear Mo species used in free-energy analysis. For further details, see Section S3.4 in the Supporting Information.

Effect of Water Co-feeding on Reduction and Stability of Mo Sites. To gauge and compare the stability of possible Mo species under varying water partial pressures, we turn to quantum mechanical calculations. First, we build a cluster model to mimic the monomeric and dimeric structures of Mo anchored ZSM-5 as full details are provided in the computational section of the Supporting Information (see Figures S61–S63 in the Supporting Information). Then, we perform an in-depth thermodynamic analysis (see the Supporting Information for the proposed reaction network) for *reduction-via-methane* (Schemes S2 and S5 in the Supporting Information) and *oxidation-via-water* (Schemes S3, S4, S6, and S7 in the Supporting Information) reactions of respective Mo states under conditions comparable to the experimental one (for more details, please see Section S3.4 in the Supporting Information). In these analyses, we focus on various Mo structures having carbide/carbene forms, since they are previously considered and proposed as MDA active sites.^{36,50–54} For both monomeric and dimeric structures, some of the carbene-containing structures (i.e., MoCH₂, Mo₂CH₂, Mo₂C₂(CH₂)₄) are more stable than carbide structures (i.e., SMOc, Mo₂C₂) under some hydrogen concentrations during the reduction process (see Figures S64 and S65 in the Supporting Information for monomeric structures and Figures S77 and S78 in the Supporting Information for dimeric structures). It is known that introducing moderate amounts of H₂O promotes the steam reforming reaction (Figure 3), which increases the overall H₂

production, whose concentration is critical for the formation and stability of carbene intermediates. Since carbene containing structures are considered crucial intermediates for coupling and further oligomerization steps,^{12,51,54,55} the improved lifetime of the catalyst with water co-feeding can be associated with increased hydrogen levels.

The free-energy profiles for oxidation and reduction reactions for monomeric systems, as a function of H₂O partial pressure at constant P_{CO} and P_{H_2} (both 10^{−2} atm), are depicted in Figure 7. All energy plots point out the exergonic nature of MoO₂ reduction reactions while oxidation of carbide and carbenes, namely, MoC, Mo(CH₂)₂, and MoCH₂, are exergonic only at significant H₂O concentrations and surpasses the reduction reactions at very high H₂O levels. Nevertheless, Mo(CH₂)₂ displays slightly different trends being prone to oxidation, even at relatively lower H₂O concentrations compared to MoC and MoCH₂. Partial oxidation of all those carbene and carbide species to MoO is the most favorable, followed by complete oxidation to MoO₂. Oxidation to Mo is also probable particularly for MoC and Mo(CH₂)₂ species, albeit thermodynamically less favored (see Figures S74a and S75a in the Supporting Information).

Next, we continued with the dimeric Mo species and applied the same thermodynamic analysis, as illustrated in Figure 8. All reduced dimeric carbide and carbene species facilitate the formation of oxo species at relatively high H₂O partial pressures when there is significant CO and H₂ in the system (both at 10^{−2} atm). As a result of oxidation, Mo₂O₅, Mo₂O₄,

and Mo_2O_3 are the most favored structures at high water concentrations (also see Figures S87a, S88a, and S89a in the Supporting Information). Oxidation from $\text{Mo}_2\text{C}_2(\text{CH}_2)_4$ and $\text{Mo}_2(\text{CH}_2)_4$ to respective Mo-oxo species is more exergonic, compared to Mo_2C_2 , because of their extremely reduced nature. In comparison to monomeric sites, oxidation of dimeric sites is far more exergonic that might indicate that polymeric Mo structures are more inclined to be oxidized. Furthermore, our analysis reveals that H_2 and CO concentrations play critical roles (see Section S3.4 in the Supporting Information). For instance, when H_2 and CO are present in negligible amounts (10^{-15} atm), oxidation reactions are far less exergonic; structures such as MoC , MoCH_2 , Mo_2C_2 bear very high stability under significantly high-water levels (see Figures S74b, S76b, and S87b in the Supporting Information). This implies that, even in the presence of high water concentrations, Mo sites lean toward reduction at the onset of the activation period (when there is no H_2 and CO formation); however, the complete reduction cannot be achieved with the formation of H_2 and CO in the reaction environment. This can be clearly deduced from the $P_{\text{H}_2\text{O}} = 0.107$ -spent sample analysis exhibiting negligible MDA yet still with some H_2 and CO production (Figure 3). Overall, markedly favorable formation of MoO , Mo_2O_4 , and Mo_2O_3 from monomeric/dimeric carbides/carbenes at high water levels points out Mo^{5+} and Mo^{4+} states as the most stable ones, which is consistent with the XPS and EPR data of the $P_{\text{H}_2\text{O}} = 0.107$ -spent sample. Detailed mechanistic investigations conducted by Guanna et al.⁵⁰ highlighted that partially reduced molybdenum sites are not as active as completely reduced carbidic sites. Thus, this explains the inhibition of MDA reaction at high water levels. Overall, DFT calculations corroborates the consistency between theory and experiment, thereby confirming the robustness of our methodology.

Effect of Water Co-feeding on Coking and Recycling.

Analyzing the coking in the spent catalysts under different humidity levels at 725 °C can provide some insight into how deactivation is being affected by water that has been co-fed. From the TG-TPO/MS experiment results, it was observed that the total coke amount on/in the catalyst is greatly reduced upon increasing the inlet water concentrations (see Table S7 in the Supporting Information), which is consistent with the catalysis performance data (Figure 4), and the N_2 physisorption analyses (see Figure S30 and Table S7 in the Supporting Information). Furthermore, from DTG and normalized $d(\text{CO}_2)/d(t)$ curves (Figures S32 and S33 in the Supporting Information), it was noticed that the peak position was shifted toward the lower temperatures upon increasing the water level. This is most probably related to the amount of coke formed (especially inside the pores) at different water levels, since there is no sharp difference in the MDA reaction mechanism in the presence of water. Next, we performed Cr-assisted TG-TPO/MS experiments on some spent samples at 725 °C in order to discriminate between internal and external coke, since chromium oxides have little influence on the oxidation of internal coke while accelerating the oxidation of the external.⁵⁶ It was realized that as the water in the inlet stream increases, the internal/external coke ratio is increasing (see Figure S34 and Table S7 in the Supporting Information), which implies that the steam-reforming reaction is more effective on the active sites located on the external surface.

Besides these, it is well-known that the coke accumulation inside the zeolite pores entails changes in unit-cell dimensions.^{57,58} In this study, we conducted principal component analysis (PCA) on a set of unit cell data (see Section S2.11.1 in the Supporting Information), derived from Pawley refinement of several catalysts acting under different conditions, to determine which parameter can better describe the catalyst structure, in terms of deactivation. As can be observed from PCA biplots (Figure 9a), the unit cell

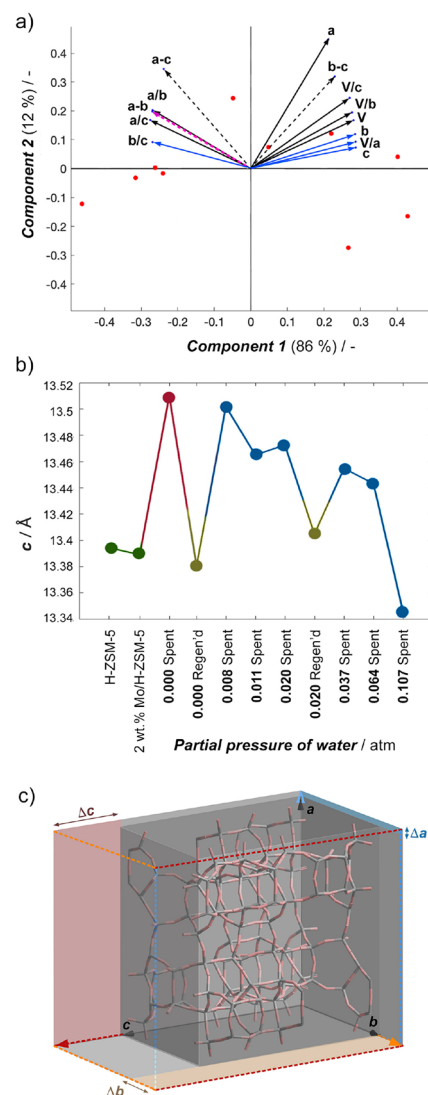


Figure 9. (a) Biplots of the principal component analysis (PCA) for unit-cell parameters in the ZSM-5 samples (fresh and after catalytic test under different conditions) derived from Pawley refinement. The principal components (component 1 and component 2) explained 98% of the total variation in unit-cell data. Red dots represent sampling data; arrows represent unit-cell parameters (black solid arrows represent active variables, black dashed arrows represent linearly dependent variables, red dashed arrows represent linearly dependent variables used as deactivation descriptors by Svelle et al.,⁵⁸ and blue solid arrows represent variables with a maximum contribution). (b) Scatter of unit-cell *c*-axis values as a response to the conditions in which ZSM-5 was treated. (c) Illustration of ZSM-5 unit-cell expansion during the deactivation of the catalyst. Among all three directions, *c* shows the strongest variance. For more details, see Section S2.11.1 in the Supporting Information.

parameters such as “ c ”, “ b/c ”, “ b ”, and “ V/a ” provide a more significant contribution to a variance of component 1. Notably, parameter c shows the greater magnitude of such deviance among others ($c > b > a$; see Figure 9c); therefore, there can be alternative descriptors for the catalyst (MFI) deactivation in place of the one (“ $a-b$ ”) suggested by Svelle et al.⁵⁸ This finding can be explained with the directions of the channels in MFI topology and bulk modulus: Since straight and (relatively narrower) sinusoidal channels are propagating along the “ b ”- and “ a ”-axes, respectively, it would be anticipated that coke accumulation would induce greater expansion of the framework in the c -direction, particularly considering its higher flexibility in comparison to other directions.⁵⁸ Also, the correlation diagrams summarize the interrelation between the coke content along with textural properties of the catalysts (see Figures S56 and S57 in the Supporting Information) and unit-cell variables, further corroborating a strong correlation of parameter c with the main characteristics of the catalyst deactivation.

The re-usability after dry and wet catalysis tests is another question. To study this, first we regenerated the $P_{\text{H}_2\text{O}} = 0.020$ and $P_{\text{H}_2\text{O}} = 0.000$ -spent catalysts under air flow at 550 °C and examined the samples with 1D ^{27}Al MAS NMR (Figure S46 in the Supporting Information), 2D ^{27}Al MQMAS NMR (Figure S47 in the Supporting Information), XRD/Pawley refinement (Figures S51 and S55 in the Supporting Information), XPS (Figure S25a in the Supporting Information), Raman (Figure S24a in the Supporting Information), and N_2 physisorption (Figure S31 in the Supporting Information). Upon regeneration, the primary characteristic features of Mo-ZSM-5 materials were mostly recovered for both cases. The catalysis tests for both regenerated samples under their corresponding conditions showed no deterioration in the overall performance (Figures S21 and S22 in the Supporting Information).

CONCLUSION

In summary, besides highlighting the benefits of limited water co-feeding on overall MDA activity, it was found out that the steam-reforming reaction also requires activated Mo sites and proceeds parallel to MDA. The most prominent outcome of this work is revealing that water is not a *game-changer* in the typical MDA reaction mechanism observed after the activation–induction period. While CO among the reforming products can involve in Koch-type carbonylation on BASs and further lead to acetal formations (which we have identified in our previous work¹² as well) or may dissociate on active Mo sites to some extent and contribute to the hydrocarbon formation,^{14,30} CD_4 – H_2O experiments showed us that hydrogen molecules have almost negligible participation in the hydrocarbon formations. However, these hydrogens, which were created because of water conversion, can thermodynamically affect the extent of de/hydrogenation, cyclization, and alkylation reactions occurring in the hydrocarbon pool. Moreover, our detailed experimental and computational studies showed that water concentration plays a key role in Mo reduction that occurs at the beginning of the process. When it exceeds the limits, only partial reduction can be achieved, which is not enough for notable methane conversion to valuable chemicals. Furthermore, the thermodynamic analysis depicts that H_2 from reforming reactions can enhance the stability of Mo-carbene structures, which are considered crucial for MDA. Therefore, there must be an elaborate

interplay between H_2 and H_2O compositions that invoke the prudent design of MDA catalyst. Beyond all of these, our statistical investigations on crystallographic features, textural properties and coke contents exhibited that the “ c ” direction of the MFI unit cell bears a close correlation with the catalyst deactivation. Altogether, our findings could help to unravel the structure–function relationship with the ultimate goal of developing techno-economically feasible catalytic processes to convert methane to aromatics.

ASSOCIATED CONTENT

Supporting Information

The Supporting Information is available free of charge at <https://pubs.acs.org/doi/10.1021/acscatal.1c02763>.

Details about catalyst preparation and experimental/theoretical techniques, characterization data, catalytic tests and results, DFT-based thermodynamic analysis (PDF)

AUTHOR INFORMATION

Corresponding Author

Jorge Gascon – KAUST Catalysis Center (KCC), Advanced Catalytic Materials, King Abdullah University of Science and Technology (KAUST), Thuwal 23955, Saudi Arabia; orcid.org/0000-0001-7558-7123; Email: jorge.gascon@kaust.edu.sa

Authors

Mustafa Çağlayan – KAUST Catalysis Center (KCC), Advanced Catalytic Materials, King Abdullah University of Science and Technology (KAUST), Thuwal 23955, Saudi Arabia

Alessandra Lucini Paioni – NMR Spectroscopy group, Bijvoet Centre for Biomolecular Research, Utrecht University, 3584 CH Utrecht, The Netherlands

Büşra Dereli – KAUST Catalysis Center (KCC), King Abdullah University of Science and Technology (KAUST), Thuwal 23955, Saudi Arabia

Genrikh Shterk – KAUST Catalysis Center (KCC), Advanced Catalytic Materials, King Abdullah University of Science and Technology (KAUST), Thuwal 23955, Saudi Arabia

Idoia Hita – KAUST Catalysis Center (KCC), Multiscale Reaction Engineering, King Abdullah University of Science and Technology (KAUST), Thuwal 23955, Saudi Arabia

Edy Abou-Hamad – Imaging and Characterization Department, Core Laboratories, King Abdullah University of Science and Technology (KAUST), Thuwal 23955, Saudi Arabia

Alexey Pustovarenko – KAUST Catalysis Center (KCC), Advanced Catalytic Materials, King Abdullah University of Science and Technology (KAUST), Thuwal 23955, Saudi Arabia

Abdul-Hamid Emwas – Imaging and Characterization Department, Core Laboratories, King Abdullah University of Science and Technology (KAUST), Thuwal 23955, Saudi Arabia

Alla Dikhtiarenko – KAUST Catalysis Center (KCC), Advanced Catalytic Materials, King Abdullah University of Science and Technology (KAUST), Thuwal 23955, Saudi Arabia; orcid.org/0000-0002-3372-2435

Pedro Castaño – KAUST Catalysis Center (KCC), Multiscale Reaction Engineering, King Abdullah University of Science and Technology (KAUST), Thuwal 23955, Saudi Arabia
Luigi Cavallo – KAUST Catalysis Center (KCC), King Abdullah University of Science and Technology (KAUST), Thuwal 23955, Saudi Arabia; orcid.org/0000-0002-1398-338X

Marc Baldus – NMR Spectroscopy group, Bijvoet Centre for Biomolecular Research, Utrecht University, 3584 CH Utrecht, The Netherlands

Abhishek Dutta Chowdhury – The Institute for Advanced Studies (IAS), Wuhan University, Wuhan 430072 Hubei, China; orcid.org/0000-0002-4121-7375

Complete contact information is available at:
<https://pubs.acs.org/10.1021/acscatal.1c02763>

Notes

The authors declare no competing financial interest.

ACKNOWLEDGMENTS

Funding for this work was provided by King Abdullah University of Science and Technology (KAUST). The authors wish to acknowledge and thank Sandra Ramirez Cherbuy for the illustration (Scheme 1). Also, we would like to thank Dr. Jullian Vittenet for his support in ICP-OES analyses. A.D.C. acknowledges the financial supports of the start-up research grant from the Institute for Advanced Studies (IAS), Wuhan University (China). M.B. and A.L.P. acknowledge the TOP-PUNT (No. 718.015.001) and a Middelgroot program (No. 700.58.102) grant supports from NWO.

REFERENCES

- (1) Zichittella, G.; Pérez-Ramírez, J. Status and Prospects of the Decentralised Valorisation of Natural Gas into Energy and Energy Carriers. *Chem. Soc. Rev.* **2021**, *50* (5), 2984–3012.
- (2) Saunio, M.; Stavert, A. R.; Poulter, B.; Bousquet, P.; Canadell, J. G.; Jackson, R. B.; Raymond, P. A.; Dlugokencky, E. J.; Houweling, S.; Patra, P. K.; et al. The Global Methane Budget 2000 - 2017. *Earth Syst. Sci. Data* **2020**, *12* (3), 1561–1623.
- (3) Schwach, P.; Pan, X.; Bao, X. Direct Conversion of Methane to Value-Added Chemicals over Heterogeneous Catalysts: Challenges and Prospects. *Chem. Rev.* **2017**, *117* (13), 8497–8520.
- (4) Gemini Process Technology: Natural Gas to Ethylene. Available via the Internet at: http://siluria.com/Products/Gemini_-_Natural_Gas_to_Ethylene (accessed April 7, 2019).
- (5) Wang, L.; Tao, L.; Xie, M.; Xu, G.; Huang, J.; Xu, Y. Dehydrogenation and Aromatization of Methane under Non-Oxidizing Conditions. *Catal. Lett.* **1993**, *21* (1–2), 35–41.
- (6) Menon, U.; Rahman, M.; Khatib, S. J. A Critical Literature Review of the Advances in Methane Dehydroaromatization over Multifunctional Metal-Promoted Zeolite Catalysts. *Appl. Catal., A* **2020**, *608*, 117870.
- (7) Kosinov, N.; Hensen, E. J. M. Reactivity, Selectivity, and Stability of Zeolite-Based Catalysts for Methane Dehydroaromatization. *Adv. Mater.* **2020**, *32*, 2002565.
- (8) Kiani, D.; Sourav, S.; Tang, Y.; Baltrusaitis, J.; Wachs, I. E. Methane Activation by ZSM-5-Supported Transition Metal Centers. *Chem. Soc. Rev.* **2021**, *50* (2), 1251–1268.
- (9) Vollmer, I.; Yarulina, I.; Kapteijn, F.; Gascon, J. Progress in Developing a Structure-Activity Relationship for the Direct Aromatization of Methane. *ChemCatChem* **2019**, *11* (1), 39–52.
- (10) Galadima, A.; Muraza, O. Advances in Catalyst Design for the Conversion of Methane to Aromatics: A Critical Review. *Catal. Surv. Asia* **2019**, *23* (3), 149–170.
- (11) *World Energy Outlook 2020*; British Petroleum, 2020.
- (12) Çağlayan, M.; Paioni, A. L.; Abou-Hamad, E.; Shterk, G.; Pustovarenko, A.; Baldus, M.; Chowdhury, A. D.; Gascon, J. Initial Carbon-Carbon Bond Formation during the Early Stages of Methane Dehydroaromatization. *Angew. Chem., Int. Ed.* **2020**, *59*, 16741–16746.
- (13) *Methane Tracker 2021*; IEA: Paris, 2021; available via the Internet at: <https://www.iea.org/reports/methane-tracker-2021>.
- (14) Yao, S.; Sun, C.; Li, J.; Huang, X.; Shen, W. A ¹³C Isotopic Study on the CO Promotion Effect in Methane Dehydroaromatization Reaction over a Mo/HMCM-49 Catalyst. *J. Nat. Gas Chem.* **2010**, *19* (1), 1–5.
- (15) Ohnishi, R.; Liu, S.; Dong, Q.; Wang, L.; Ichikawa, M. Catalytic Dehydrocondensation of Methane with CO and CO₂ toward Benzene and Naphthalene on Mo/HZSM-5 and Fe/Co-Modified Mo/HZSM-5. *J. Catal.* **1999**, *182* (1), 92–103.
- (16) Ma, H.; Kojima, R.; Kikuchi, S.; Ichikawa, M. Effective Coke Removal in Methane to Benzene (MTB) Reaction on Mo/HZSM-5 Catalyst by H₂ and H₂O Co-Addition to Methane. *Catal. Lett.* **2005**, *104* (1–2), 63–66.
- (17) Yuan, S.; Li, J.; Hao, Z.; Feng, Z.; Xin, Q.; Ying, P.; Li, C. The Effect of Oxygen on the Aromatization of Methane over the Mo/HZSM-5 Catalyst. *Catal. Lett.* **1999**, *63* (73–77), 73–77.
- (18) Skutil, K.; Taniewski, M. Some Technological Aspects of Methane Aromatization (Direct and via Oxidative Coupling). *Fuel Process. Technol.* **2006**, *87* (6), 511–521.
- (19) Liu, S.; Ohnishi, R.; Ichikawa, M. Promotional Role of Water Added to Methane Feed on Catalytic Performance in the Methane Dehydroaromatization Reaction on Mo/HZSM-5 Catalyst. *J. Catal.* **2003**, *220* (1), 57–65.
- (20) Liu, Z.; Nutt, M. A.; Iglesia, E. The Effects of CO₂, CO and H₂ Co-Reactants on Methane Reactions Catalyzed by Mo/ZSM-5. *Catal. Lett.* **2002**, *81* (3–4), 271–279.
- (21) Tan, P. L.; Leung, Y. L.; Lai, S. Y.; Au, C. T. Methane Aromatization over 2 Wt% Mo/HZSM-5 in the Presence of O₂ and NO. *Catal. Lett.* **2002**, *78*, 251–258.
- (22) Aritani, H.; Shibasaki, H.; Orihara, H.; Nakahira, A. Methane Dehydroaromatization over Mo-Modified H-MFI for Gas to Liquid Catalysts. *J. Environ. Sci.* **2009**, *21* (6), 736–740.
- (23) Chen, M.; Song, Y.; Liu, B.; Liu, X.; Xu, Y.; Zhang, Z. Experimental Investigation of the Promotion Effect of CO on Catalytic Behavior of Mo/HZSM-5 Catalyst in CH₄ Dehydroaromatization at 1073 K. *Fuel* **2020**, *262*, 116674.
- (24) De Wispelaere, K.; Wondergem, C. S.; Ensing, B.; Hemelsoet, K.; Meijer, E. J.; Weckhuysen, B. M.; Van Speybroeck, V.; Ruiz-Martínez, J. Insight into the Effect of Water on the Methanol-to-Olefins Conversion in H-SAPO-34 from Molecular Simulations and in Situ Microspectroscopy. *ACS Catal.* **2016**, *6* (3), 1991–2002.
- (25) Ma, S.; Guo, X.; Zhao, L.; Scott, S.; Bao, X. Recent Progress in Methane Dehydroaromatization: From Laboratory Curiosities to Promising Technology. *J. Energy Chem.* **2013**, *22* (1), 1–20.
- (26) Ma, H.; Kojima, R.; Kikuchi, S. Hydrogen Effect on Coke Removal and Catalytic Performance in Pre-Carburization and Methane Dehydro-Aromatization Reaction on Mo/HZSM-5. *J. Nat. Gas Chem.* **2005**, *14*, 129–139.
- (27) Bedard, J.; Hong, D. Y.; Bhan, A. CH₄ Dehydroaromatization on Mo/H-ZSM-5:1. Effects of Co-Processing H₂ and CH₃COOH. *J. Catal.* **2013**, *306*, 58–67.
- (28) Bedard, J.; Hong, D. Y.; Bhan, A. Co-Processing CH₄ and Oxygenates on Mo/H-ZSM-5:2. CH₄-CO₂ and CH₄-HCOOH Mixtures. *Phys. Chem. Chem. Phys.* **2013**, *15* (29), 12173–12179.
- (29) Bedard, J.; Hong, D. Y.; Bhan, A. C to H Effective Ratio as a Descriptor for Co-Processing Light Oxygenates and CH₄ on Mo/H-ZSM-5. *RSC Adv.* **2014**, *4* (90), 49446–49448.
- (30) Vollmer, I.; Van Der Linden, B.; Ould-Chikh, S.; Aguilar-Tapia, A.; Yarulina, I.; Abou-Hamad, E.; Sneider, Y. G.; Olivos Suarez, A. I.; Hazemann, J. L.; Kapteijn, F.; Gascon, J. On the Dynamic Nature of Mo Sites for Methane Dehydroaromatization. *Chem. Sci.* **2018**, *9* (21), 4801–4807.

- (31) Hunt, J.; Ferrari, A.; Lita, A.; Crosswhite, M.; Ashley, B.; Stiegman, A. E. Microwave-Specific Enhancement of the Carbon-Carbon Dioxide (Boudouard) Reaction. *J. Phys. Chem. C* **2013**, *117*, 26871–26880.
- (32) Porosoff, M. D.; Yang, X.; Boscoboinik, J. A.; Chen, J. G. Molybdenum Carbide as Alternative Catalysts to Precious Metals for Highly Selective Reduction of CO₂ to CO. *Angew. Chem., Int. Ed.* **2014**, *53* (26), 6705–6709.
- (33) Arora, S. S.; Nieskens, D. L. S.; Malek, A.; Bhan, A. Lifetime Improvement in Methanol-to-Olefins Catalysis over Chabazite Materials by High-Pressure H₂ Co-Feeds. *Nat. Catal.* **2018**, *1* (9), 666–672.
- (34) Meusinger, J.; Corma, A. Activation of Hydrogen on Zeolites: Kinetics and Mechanism of n-Heptane Cracking on H-ZSM-5 Zeolites under High Hydrogen Pressure. *J. Catal.* **1995**, *152* (1), 189–197.
- (35) Qi, G.; Wang, Q.; Xu, J.; Deng, F. Solid-State NMR Studies of Internuclear Correlations for Characterizing Catalytic Materials. *Chem. Soc. Rev.* **2021**, *50* (15), 8382–8399.
- (36) Lezcano-González, I.; Oord, R.; Rovezzi, M.; Glatzel, P.; Botchway, S. W.; Weckhuysen, B. M.; Beale, A. M. Molybdenum Speciation and Its Impact on Catalytic Activity during Methane Dehydroaromatization in Zeolite ZSM-5 as Revealed by Operando X-Ray Methods. *Angew. Chem., Int. Ed.* **2016**, *55* (17), 5215–5219.
- (37) Razdan, N. K.; Kumar, A.; Foley, B. L.; Bhan, A. Influence of Ethylene and Acetylene on the Rate and Reversibility of Methane Dehydroaromatization on Mo/H-ZSM-5 Catalysts. *J. Catal.* **2020**, *381*, 261–270.
- (38) Stanciakova, K.; Weckhuysen, B. M. Water-Active Site Interactions in Zeolites and Their Relevance in Catalysis. *Trends Chem.* **2021**, *3* (6), 456–468.
- (39) Pines, A.; Gibby, M. G.; Waugh, J. S. Proton-Enhanced Nuclear Induction Spectroscopy: a Method for High Resolution Nmr of Dilute Spins in Solids. *J. Chem. Phys.* **1972**, *56* (4), 1776–1777.
- (40) Morris, G. A.; Freeman, R. Enhancement of Nuclear Magnetic Resonance Signals by Polarization Transfer. *J. Am. Chem. Soc.* **1979**, *101* (3), 760–762.
- (41) Gabrienko, A. A.; Arzumanov, S. S.; Toktarev, A. V.; Danilova, I. G.; Prosvirnin, I. P.; Kriventsov, V. V.; Zaikovskii, V. I.; Freude, D.; Stepanov, A. G. Different Efficiency of Zn²⁺ and ZnO Species for Methane Activation on Zn-Modified Zeolite. *ACS Catal.* **2017**, *7* (3), 1818–1830.
- (42) Luzgin, M. V.; Toktarev, A. V.; Parmon, V. N.; Stepanov, A. G. Coaromatization of Methane with Propane on Mo-Containing Zeolite H-BEA: A Solid-State NMR and GC-MS Study. *J. Phys. Chem. C* **2013**, *117* (44), 22867–22873.
- (43) Chakarova, K.; Drenchev, N.; Hadjiivanov, K. FTIR Evidence of Different Bonding of Methane to OH Groups on H-ZSM-5, HY, and SiO₂. *J. Phys. Chem. C* **2012**, *116* (32), 17101–17109.
- (44) Khaliullin, R. Z.; Bell, A. T.; Kazansky, V. B. An Experimental and Density Functional Theory Study of the Interactions of CH₄ with H-ZSM-5. *J. Phys. Chem. A* **2001**, *105* (45), 10454–10461.
- (45) Bowers, G. M.; Schaef, H. T.; Miller, Q. R. S.; Walter, E. D.; Burton, S. D.; Hoyt, D. W.; Horner, J. A.; Loring, J. S.; McGrail, B. P.; Kirkpatrick, R. J. ¹³C Nuclear Magnetic Resonance Spectroscopy of Methane and Carbon Dioxide in a Natural Shale. *ACS Earth Sp. Chem.* **2019**, *3* (3), 324–328.
- (46) Chowdhury, A. D.; Houben, K.; Whiting, G. T.; Mokhtar, M.; Asiri, A. M.; Al-Thabaiti, S. A.; Basahel, S. N.; Baldus, M.; Weckhuysen, B. M. Initial Carbon-Carbon Bond Formation during the Early Stages of the Methanol-to-Olefin Process Proven by Zeolite-Trapped Acetate and Methyl Acetate. *Angew. Chem., Int. Ed.* **2016**, *55* (51), 15840–15845.
- (47) Guisnet, M. “Coke” Molecules Trapped in the Micropores of Zeolites as Active Species in Hydrocarbon Transformations. *J. Mol. Catal. A: Chem.* **2002**, *182–183*, 367–382.
- (48) Bodenhausen, G.; Ruben, D. J. Natural Abundance Nitrogen-15 NMR by Enhanced Heteronuclear Spectroscopy. *Chem. Phys. Lett.* **1980**, *69* (1), 185–189.
- (49) Bax, A.; Summers, M. F. ¹H and ¹³C Assignments from Sensitivity-Enhanced Detection of Heteronuclear Multiple-Bond Connectivity by 2D Multiple Quantum NMR. *J. Am. Chem. Soc.* **1986**, *108* (8), 2093–2094.
- (50) Li, G.; Vollmer, I.; Liu, C.; Gascon, J.; Pidko, E. A. Structure and Reactivity of the Mo/ZSM-5 Dehydroaromatization Catalyst: An Operando Computational Study. *ACS Catal.* **2019**, *9*, 8731–8737.
- (51) Zhou, D.; Zuo, S.; Xing, S. Methane Dehydrogenation and Coupling to Ethylene over a Mo/HZSM-5 Catalyst: A Density Functional Theory Study. *J. Phys. Chem. C* **2012**, *116*, 4060–4070.
- (52) Xing, S.; Zhou, D.; Cao, L.; Li, X. Density Functional Theory Study on Structure of Molybdenum Carbide and Catalytic Mechanism for Methane Activation over ZSM-5 Zeolite. *Cuihua Xuebao/Chin. J. Catal.* **2010**, *31* (4), 415–422.
- (53) Gao, W.; Qi, G.; Wang, Q.; Wang, W.; Li, S.; Hung, I.; Gan, Z.; Xu, J.; Deng, F. Dual Active Sites on Molybdenum/ZSM-5 Catalyst for Methane Dehydroaromatization: Insights from Solid-State NMR Spectroscopy. *Angew. Chem., Int. Ed.* **2021**, *60*, 10709–10715.
- (54) Sij, M.; Oudghiri-Hassani, H.; Maltis, C.; McBreen, P. H. Thermally Stable Alkylidene Groups on the Surface of β -Mo²⁺: Relevance to Methane Aromatization and Olefin-Metathesis Catalysis. *J. Phys. Chem. C* **2007**, *111* (4), 1725–1732.
- (55) Soulivong, D.; Norsic, S.; Taoufik, M.; Copéret, C.; Thivolle-Cazat, J.; Chakka, S.; Basset, J. M. Non-Oxidative Coupling Reaction of Methane to Ethane and Hydrogen Catalyzed by the Silica-Supported Tantalum Hydride: (\equiv SiO)₂Ta-H. *J. Am. Chem. Soc.* **2008**, *130*, 5044–5045.
- (56) Wang, T.; Chen, M.; Liu, X.; Zhang, Z. G.; Xu, Y. Distinguishing External and Internal Coke Depositions on Micron-Sized HZSM-5: Via Catalyst-Assisted Temperature-Programmed Oxidation. *New J. Chem.* **2019**, *43* (35), 13938–13946.
- (57) Goetze, J.; Yarulina, I.; Gascon, J.; Kapteijn, F.; Weckhuysen, B. M. Revealing Lattice Expansion of Small-Pore Zeolite Catalysts during the Methanol-to-Olefins Process Using Combined Operando X-Ray Diffraction and UV-Vis Spectroscopy. *ACS Catal.* **2018**, *8* (3), 2060–2070.
- (58) Rojo-Gama, D.; Nielsen, M.; Wragg, D. S.; Dyballa, M.; Holzinger, J.; Falsig, H.; Lundegaard, L. F.; Beato, P.; Brogaard, R. Y.; Lillerud, K. P.; Olsbye, U.; Svelle, S. A Straightforward Descriptor for the Deactivation of Zeolite Catalyst H-ZSM-5. *ACS Catal.* **2017**, *7* (12), 8235–8246.